Constitutive Model of Concrete Simultaneously Confined by FRP and Steel for Finite-Element Analysis of FRP-Confined RC Columns

Diogo Zignago[1]; Michele Barbato, M.ASCE[2]; and Dan Hu[3]

Abstract: This paper presents a confined concrete material constitutive model for use in finite-element analysis, which is able to model accurately the combined confinement effect of fiber-reinforced polymers (FRP) and internal steel reinforcement on the structural monotonic, cyclic, and/or dynamic response of reinforced concrete (RC) columns confined with externally wrapped FRP. The proposed material constitutive model for FRP-and-steel confined concrete explicitly models the simultaneous confinement produced by FRP and steel on the core concrete to predict the combined effect on the structural response of circular RC columns. This modified material model is combined with a force-based frame element to predict numerically the load-carrying capacity of FRP-confined RC columns subjected to different loading conditions. Numerical simulations are compared to experimental test data available in the literature and published by different authors. The numerically simulated responses agree very well with the corresponding experimental results. The proposed model is found to predict the ultimate load for FRP-confined RC circular columns with better accuracy than models that do not consider the simultaneous confinement effects on FRP and steel, particularly for columns subjected to concentric axial loads. **DOI: 10.1061/(ASCE)CC.1943-5614.0000902.**

Author keywords: Fiber-reinforced polymers; Reinforced concrete; Confinement; Nonlinear material behavior; Finite-element method.

Introduction

Existing reinforced concrete (RC) structures often need rehabilitation or strengthening due to inappropriate design or construction, modification of the use and of the corresponding design loads, and damage caused by environmental factors and/or extraordinary loading events. Retrofitting and repairing of damaged and/or inappropriately designed concrete structures using externally bonded fiber-reinforced polymers (FRP) have been proved to be effective alternatives to other types of strengthening techniques (e.g., steel jackets), presenting some advantages like excellent corrosion resistance, fire resistance, ease of transportation and installation, and high strength-to-weight ratio of FRP sheets, which leads to a minimum increase of the structure's weight and dimensions (Bakis et al. 2002; Cheng and Karbhari 2006; Basalo et al. 2012). This retrofit method has become more common during the last few decades and has been widely applied specially to columns of bridges and buildings (Seible et al. 1997; Flaga 2000; Pantelides et al. 2000; Mertz et al. 2003; Motavalli and Czaderski 2007).

The amount of longitudinal and transverse reinforcement in RC columns must satisfy minimum design code requirements in terms of flexural and shear strength. As a result, RC columns that need to be retrofitted with FRP laminates also contain longitudinal and transverse steel reinforcement. Thus, in these retrofitted RC columns, a significant portion of the concrete is subjected to two simultaneous confinement actions: the confinement due to FRP plates/sheets and the confinement due to internal (longitudinal and transverse) steel reinforcement. FRP jacketing of RC columns exerts a linearly increasing confining pressure up to rupture on the concrete due to its lateral dilation when loaded, while the internal reinforcing steel is responsible for a constant confining pressure after yielding (Spoelstra and Monti 1999). Both types of confinement enhance the seismic performance of the RC column, improving the concrete compressive strength and thus the ductility of the member, and making FRP-wrapped RC columns more suitable, e.g., to undergo large lateral displacements imposed by severe earthquakes.

The majority of the stress-strain models available in the literature to model FRP-confined concrete do not account for the influence of the existing internal steel reinforcement on the mechanical behavior of concrete confined through externally bonded FRP laminates (Spoelstra and Monti 1999; Fardis and Khalili 1982; Mirmiran and Shahawy 1996; Karbhari and Gao 1997; Samaan et al. 1998; Toutanji 1999; Xiau and Wu 2000; Fam and Rizkalla 2001; Shao et al. 2006). Kawashima et al. (2000) proposed two different confined concrete stress-strain models: one for concrete confined with carbon FRP only and one for concrete confined simultaneously by carbon FRP and transverse steel ties. A regression analysis, based on the experimental results obtained through two-phase loading tests on RC specimens with circular and rectangular sections, was used to calibrate the parameters needed to define these two stress-strain confined concrete models. The model was validated by comparing the envelope curves of the lateral force versus lateral displacement response of six specimens with the corresponding curves analytically obtained through a fiber analysis based on the developed equations. Li et al. (2003) developed a constitutive model for carbon FRP-confined concrete. The peak

[1]Graduate Research Assistant, Dept. of Civil and Environmental Engineering, Univ. of California Davis, One Shields Ave., Davis, CA 95616. Email: zignago@ucdavis.edu

[2]Professor, Dept. of Civil and Environmental Engineering, Univ. of California Davis, One Shields Ave., Davis, CA 95616 (corresponding author). Email: mbarbato@ucdavis.edu

[3]Structural Project Engineer, ATI Architects and Engineers, 4750 Willow Rd., Pleasanton, CA 94588. Email: chu@atiae.com

Note. This manuscript was submitted on March 5, 2018; approved on June 22, 2018; published online on October 15, 2018. Discussion period open until March 15, 2019; separate discussions must be submitted for individual papers. This paper is part of the ***Journal of Composites for Construction***, © ASCE, ISSN 1090-0268.

strength of the confined concrete was derived from the Mohr-Coulomb failure criterion, whereas the strain at the peak strength was obtained from a regression analysis based on experimental compression tests. This material constitutive model was modified to model concrete confined by both steel reinforcement and carbon FRP. In the modified model, the strength of the confined concrete was obtained by summing three independent contributions, i.e., (1) the unconfined concrete strength, (2) the strength increment due to the confinement produced by the carbon FRP, and (3) the strength increment due to the confinement produced by the steel reinforcement. This modified confined concrete model was also verified by comparisons with experimental tests. Using a similar approach to that employed in Li et al. (2003), Ilki et al. (2008) derived a set of empirical equations to describe the stress-strain response of concrete confined simultaneously by steel and FRP and used this new model to successfully predict the compressive strength and corresponding axial deformation of FRP jacketed columns. Pellegrino and Modena (2010) investigated the interaction mechanisms between internal steel reinforcement and external FRP confinement. An analytical model was proposed to describe the stress-strain monotonic envelope response of FRP confined elements with circular and rectangular cross-sections with or without internal steel reinforcement. The model was found to agree well with experimental results available in the literature. Hu and Seracino (2014) developed an analysis-oriented FRP-confined model that also accounts for the confinement produced by internal steel reinforcement. This model uses a stress-strain curve proposed by Popovics (1973), in which the peak strength of the confined material is obtained as the summation of the peak strength of the unconfined material and the strength contributions due to steel and FRP confinement considered as independent. These contributions are based on the models proposed by Mander et al. (1988) for the steel confinement and Teng et al. (2007) for the FRP confinement. Shirmohammadi et al. (2015) also developed a model that predicts the monotonic stress-strain relationship of confined concrete, considering the double confinement. The model was implemented in a fiber-based moment-curvature analysis and showed better agreement with experimental results than other tested models. Ismail et al. (2017) modified a design-oriented model for FRP-confined concrete by adding the effect of steel confinement through a shift in the stress-strain curve without any modification of the stiffness.

This paper extends an analysis-oriented material constitutive model of FRP-confined concrete, originally developed by Spoelstra and Monti (1999) and applied to finite-element (FE) analysis of FRP-retrofitted columns by Hu and Barbato (2014). This modified model accounts for the simultaneous confinement effects of internal steel reinforcement and externally bonded FRP laminates on the structural monotonic, cyclic, and/or dynamic response of FRP-retrofitted RC columns. The proposed material constitutive model is validated against experimental data available in the literature for the structural response of FRP-retrofitted RC columns with circular cross-section and subjected to different loading conditions. The structural response of these columns was numerically predicted using the proposed material model in conjunction with a force-based frame FE with fiber-discretized sections (Spacone et al. 1996; Neuenhofer and Filippou 1997; Scott and Fenves 2006; Hu and Barbato 2014).

Research Relevance

The proposed material constitutive model enables a computationally efficient approach to model the simultaneous confinement mechanisms of reinforcing steel and FRP within the cross-section of an RC column. In conjunction with the fiber-section force-based frame element used in this research, it can provide structural analysts with a practical tool for performance assessment and design of FRP retrofit of deficient RC columns. The proposed model is particularly suitable for accurate and computationally efficient modeling of large-scale structures (e.g., buildings and bridges) subject to static and dynamic loadings, as well as for reliability assessment of real-world structures. Moreover, the accurate modeling of the simultaneous steel-FRP confinement effects on concrete could improve the efficiency of columns' FRP retrofit by reducing the conservativeness of models that neglect the steel's confining effect and by providing better estimates of the structural component ductility after retrofit, which is a crucial ingredient, e.g., for performance-based design of RC bridges.

Material Constitutive Model for Concrete Confined with Steel and FRP

The material constitutive model proposed by Spoelstra and Monti (1999) (referred to as the SM model hereinafter) provides an axial stress-axial strain curve based on an iterative numerical procedure that enforces equilibrium and compatibility between the radial stress and deformation for the confined concrete and the axial stress and hoop deformation for the confinement devices. The SM model is suitable to predict the structural behavior of concrete confined with externally bonded FRP, steel jackets, or internal steel reinforcement. However, this model does not consider the interaction effects due to simultaneous confinement actions of steel and FRP and is valid only for monotonic loading of the confined concrete.

This study proposes a modified SM (mSM) confined concrete model that (1) can account for simultaneous confinement by steel and FRP in determining the monotonic envelope of the confined concrete, and (2) possesses simple unloading and reloading rules that allow the use of the material constitutive model under general loading conditions. The mSM model is based on the same iterative procedure used by the SM model, but it differs from it for the calculation of the total confinement pressure. This new model is described in the following subsections. It is also noted here that both the SM and mSM models assume that the confined concrete has zero stress and zero stiffness in tension, i.e., they neglect tension stiffening because the focus of this study is on the ultimate behavior of columns. However, tension stiffening (Lin 2010) can be easily integrated into the proposed material constitutive model.

Monotonic Envelope of the Stress-Strain Curve

The mSM model evaluates the lateral confinement pressure as the sum of the confinement pressure due to the externally bonded FRP and internal transverse steel reinforcement. This approach differs from that used in most of the previous studies (Li et al. 2003; Ilki et al. 2008; Pellegrino and Modena 2010; Hu and Seracino 2014), which considers the sum of independent strength increments due to the confinement action of each material (steel and FRP).

The total confinement pressure, f_l', for the mSM model is calculated as follows:

$$f_l' = f_{l,\text{steel}} + f_{l,\text{FRP}} = \frac{1}{2} \cdot k_s \cdot \rho_s \cdot \sigma_s + \frac{1}{2} \cdot k_f \cdot \rho_f \cdot \sigma_f \qquad (1)$$

The term $f_{l,\text{steel}}$ in Eq. (1) represents the confinement action due to the transverse reinforcement steel, where k_s = steel confinement effectiveness coefficient (Mander et al. 1988), ρ_s = transverse steel reinforcement ratio defined as

$$\rho_s = \frac{4 \cdot A_{st}}{s \cdot d_c} \tag{2}$$

with A_{st} = cross-sectional area of a transverse reinforcing stirrup/spiral, s = clear distance between adjacent hoops or spiral turns, d_c = diameter of the confined concrete core, and σ_s = stress of the transverse reinforcing steel. The stress of the transverse reinforcing steel is given by

$$\sigma_s = \begin{cases} E_s \cdot \varepsilon_l & \text{for } \max(\varepsilon_l) < \varepsilon_y \\ f_{yt} & \text{for } \varepsilon_y \le \max(\varepsilon_l) < \varepsilon_{su} \\ 0 & \text{for } \max(\varepsilon_l) \ge \varepsilon_{su} \text{ or } \varepsilon_l < 0 \end{cases} \tag{3}$$

where E_s = elastic modulus of the transverse reinforcing steel, f_{yt} = yield strength of the transverse reinforcing steel, ε_y = yield strain of the transverse reinforcing steel, ε_{su} = rupture strain of the transverse reinforcing steel, and ε_l = lateral strain.

The term $f_{l,\text{FRP}}$ in Eq. (1) represents the confinement action due to the externally bonded FRP, where k_f = FRP confinement effectiveness coefficient (Saadatmanesh et al. 1994), ρ_f = FRP volume ratio defined as

$$\rho_f = \frac{4 \cdot t_f}{D} \tag{4}$$

with t_f = thickness of the jacket, D = diameter of the FRP jacket/sheet, and

$$\sigma_f = \begin{cases} E_f \cdot \varepsilon_l & \text{for } \max(\varepsilon_l) < \varepsilon_{f,\text{rup}} \\ 0 & \text{for } \max(\varepsilon_l) \ge \varepsilon_{f,\text{rup}} \text{ or } \varepsilon_l < 0 \end{cases} \tag{5}$$

where $\varepsilon_{f,\text{rup}} = \xi_f \cdot \varepsilon_{fu} = \xi_f \cdot f_{fu}/E_f$ = rupture strain of FRP, ξ_f = efficiency factor, ε_{fu} = ultimate strain from coupons tests, f_{fu} = ultimate strength of the FRP material from coupons tests, and E_f = elastic modulus of the FRP.

The axial stress-axial strain relation is calculated incrementally through the iterative procedure described in Spoelstra and Monti (1999), in which the calculation of f_l' is performed according to Eq. (1). The confining pressure for concrete confined simultaneously by steel and FRP is shown in Fig. 1 as a function of the radial strain. Typical monotonic axial stress-strain response curves for the SM model and the mSM model are compared in Fig. 2. As expected, the stress achieved in the mSM model for a given strain is higher than that in the SM model and depends on the amount and

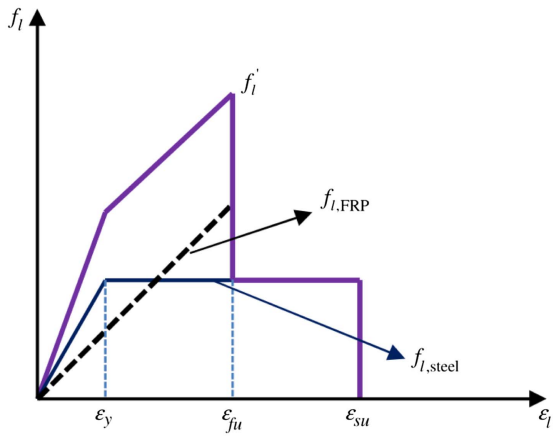

Fig. 1. Confinement pressure acting on concrete that is simultaneously confined by steel and FRP.

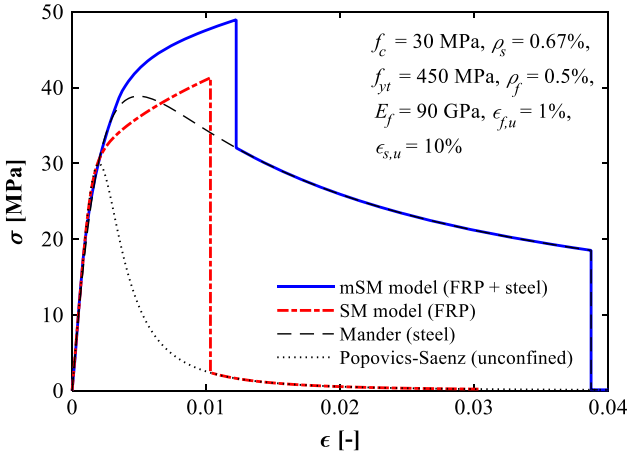

Fig. 2. Monotonic envelopes for the stress-strain relations obtained using different models and same underlying concrete properties.

configuration of confining steel. It is also noted that the peak strength (corresponding to the FRP failure) occurs at different levels of strains, with the mSM model achieving its peak strength at higher strain.

Fig. 2 also plots the stress-strain curves corresponding to the steel-confined concrete model proposed by Mander et al. (1988) and the Popovics-Saenz model for unconfined concrete (Popovics 1973; Balan et al. 1997) with the same underlying properties. It is observed that, after the FRP failure (i.e., when only the confinement from the transverse steel reinforcement is active), the mSM model reduces to the Mander's model, until the concrete lateral strain ε_l reaches the rupture strain of the transverse reinforcing steel ε_{su}, after which the mSM model reduces to residual stress of the unconfined curve. On the other hand, the SM model reduces directly to the unconfined curve as soon as the confining FRP reaches its ultimate strain.

The description provided here implies that the FRP confining material reaches failure before the confining steel, which is the most common case in practice. However, it is noteworthy that the proposed model accounts also for the less likely cases in which the confining steel reaches its ultimate strain before the confining FRP. In these cases, the mSM model first reduces to the SM model when the steel fails, and then to the Popovics-Saenz model when also the FRP fails.

Hysteretic Behavior of the Stress-Strain Curve

The hysteretic behavior of the mSM model is described by linear hysteretic unloading/reloading branches that are defined based on a set of experimental tests conducted by Barbato et al. (2003). The proposed model does not model strength deterioration due to the cumulative damage produced by repeated hysteresis loops, the effect of which was found to be very small in the experimental results. However, this effect could be added by introducing a cumulative damage parameter [e.g., see Fardis et al. (1983)]. The stiffness degradation due to the propagation of internal cracks for increasing plastic strain is considered in the calculation of the reloading stiffness, E_{rel}, and is based on the model developed by Imran and Pantazopoulou (1996). It is noted here that the original SM model consisted only of a monotonic envelope; that is, it did not consider the hysteretic response of FRP-confined concrete. The hysteretic behavior developed in this study for the mSM model is adopted also for the SM model, which is thus extended to allow

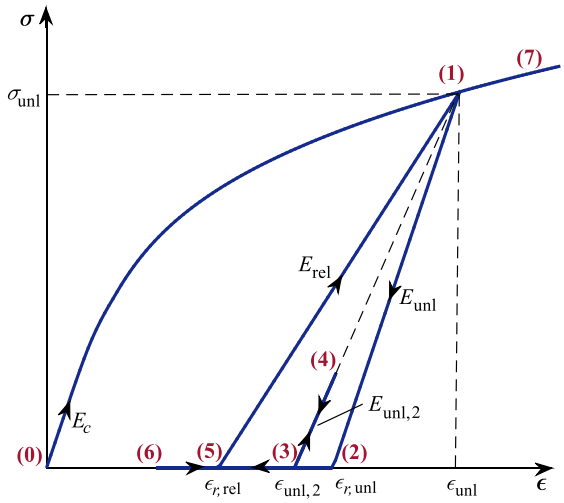

Fig. 3. Hysteretic behavior proposed for the mSM model.

the numerical analysis of the cyclic behavior of FRP-confined concrete.

Fig. 3 illustrates the unloading/reloading rules of the proposed hysteretic model by representing compression stress and strain as positive quantities for clarity's sake. Starting from a virgin material condition with zero stress and strain [point (0) in Fig. 3], the constitutive model follows the monotonic envelope for increasing compression strain up to point (1) defined by axial stress σ_{unl} and axial strain ε_{unl} where the unloading (i.e., decreasing compression strain) starts by following a straight line with a slope equal to the initial stiffness of concrete, $E_{\text{unl}} = E_c$, until zero stress is reached at a residual strain, $\varepsilon_{r,\text{unl}}$, corresponding to point (2) in Fig. 3. When the unloading initiates from the monotonic envelope, history variables representing the unrecoverable plastic strain, $\varepsilon_{r,\text{rel}}$ [corresponding to the axial strain at point (5) in Fig. 3], and the corresponding reloading stiffness, E_{rel} are evaluated as:

$$\varepsilon_{r,\text{rel}} = \varepsilon_{\text{unl}} - \frac{\sigma_{\text{unl}}}{E_{\text{rel}}} \tag{6}$$

$$E_{\text{rel}} = \frac{E_c}{(1 + 2 \cdot \alpha \cdot \varepsilon_{l,\text{unl}})} \tag{7}$$

where $\alpha = 20$ (Imran and Pantazopoulou 1996) and $\varepsilon_{l,\text{unl}}$ = lateral strain coordinate of unloading point on the envelope [point (1)]. Unless the axial strain reduces to values smaller than $\varepsilon_{r,\text{unl}}$, any reloading/unloading with strain values between $\varepsilon_{r,\text{unl}}$ and ε_{unl} happens along the straight line contained between points (1) and (2). For strain values smaller than $\varepsilon_{r,\text{unl}}$, the unloading follows a zero stress line. If a reloading occurs and the inversion point corresponds to an axial strain contained between $\varepsilon_{r,\text{rel}}$ and $\varepsilon_{r,\text{unl}}$ [i.e., point (3) in Fig. 3], the stress-strain relation follows a straight line pointing to the inversion point on the monotonic envelope [i.e., point (1)], which is defined by a slope $E_{\text{unl},2}$ given by:

$$E_{\text{unl},2} = \frac{\sigma_{\text{unl}}}{\varepsilon_{\text{unl}} - \varepsilon_{\text{unl},2}} \tag{8}$$

in which $\varepsilon_{\text{unl},2}$ denotes the new inversion point from negative strain increment to positive strain increment, the value of which is used to update history variable $\varepsilon_{r,\text{unl}}$ [with the line between points (1) and (3) effectively replacing the line between points (1) and (2) as the unloading/reloading path]. If the strain increment again changes direction [e.g., at point (4)], the hysteretic behavior follows the unloading/reloading rules previously described until the strain becomes smaller than $\varepsilon_{r,\text{rel}}$, after which no further degradation of the plastic strain recovery is allowed. This assumption implies that any reloading/unloading cycle occurring afterward [e.g., at point (6)] follows a zero stress line for any strain value smaller than $\varepsilon_{r,\text{rel}}$ (including negative values corresponding to tension strains), or the straight line between points (1) and (5) for strain values contained between $\varepsilon_{r,\text{rel}}$ and ε_{unl}. Finally, if during a reloading phase the strain becomes larger than ε_{unl} [e.g., point (7) in Fig. 3], the stress-strain relation follows again the monotonic envelope and all history variables governing the unloading/reloading behavior are reset to their initial zero values. It is noted here that this proposed hysteretic behavior is identical for any portion of the monotonic envelope, including early stages during which both FRP and steel confinements are active, the phases during which only FRP or only steel confinement is active (because one of the two has failed), and the phase in which the concrete is unconfined (i.e., when both FRP and steel have failed).

Computer Implementation and Finite-Element Formulation

The proposed material constitutive model was implemented in FEDEASLab (Filippou and Constantinides 2004), a Matlab-based (MathWorks 1997) program appropriate for linear and nonlinear, static and dynamic structural analysis. The mSM constitutive model was used to describe the stress-strain response of confined concrete fibers in a two-node one-dimensional force-based frame FE with fiber sections (Hu and Barbato 2014; Spacone et al. 1996). In particular, each section is discretized into concrete core fibers (simultaneously confined by steel and FRP and modeled using the newly developed mSM model), concrete cover fibers (confined only by FRP, for which the mSM model reduces to the SM model), and steel fibers, which are modeled using the model by Menegotto and Pinto (1973) as extended in Filippou et al. (1983) to include isotropic hardening effects. The frame FE is based on the Euler-Bernoulli beam theory with small deformations, and its element state determination employs the noniterative algorithm (Neuenhofer and Filippou 1997).

It is pointed out here that any selection of FE formulation (e.g., ordinary displacement-based frame elements or a single force-based frame element), numerical integration of section response (e.g., Gauss-Legendre or Gauss-Lobatto integration), and material constitutive models for steel fibers can be used in conjunction with the material constitutive model presented in this paper, as long as a fiber-section approach is employed. Based on the authors' experience, the numerical integration scheme using five Gauss-Lobatto integration points in conjunction with force-based elements provides the best compromise between computational cost and accuracy for the majority of the cases. However, when there is a formation of a plastic hinge in the member (e.g., in correspondence of large lateral tip displacements of cantilever beams), the strain-softening behavior of the concrete can cause a localization issue and loss of objectivity in force-based elements, making their postpeak responses dependent on the number of integration points considered in the integration scheme (Coleman and Spacone 2001). This loss of response objectivity is controlled by the integration weight of the integration point closest to the plastic hinge formation, which corresponds to the strain-softening region assumed by the FE model and not necessarily to the actual plastic hinge length of the physical member. It is worth noting that this localization issue occurs also when displacement-based elements are used to model structural members with softening behavior, in which case

it is controlled by the length of the FE that is closest to the plastic hinge formation (Coleman and Spacone 2001). In order to solve this issue, several regularization techniques were suggested in the literature (Coleman and Spacone 2001; Scott and Fenves 2006). In this study, for columns subjected to a combination of axial and lateral loads, for which plastic hinge formation was expected in correspondence of large lateral loads, the force-based beam-column element developed by Scott and Fenves (2006) was adopted. This element's formulation employs a plastic hinge integration method to overcome the nonobjectivity problem of force-based elements' response due to localization for softening structures. This element considers a plastic hinge with nonlinear behavior at each end of the element, whereas the remaining portion of the element has a linear elastic behavior. The length of the plastic hinge was assumed equal to the experimentally observed plastic hinge length (when this information was available in the literature) or estimated based on Paulay and Priestley (1992) (when this information was not reported in the literature).

Model Validation through Comparison of Numerical Estimates and Experimental Results

The proposed material constitutive model was validated through a comparison between an extensive experimental database obtained from existing literature and numerical simulation of the FE response of circular RC columns retrofitted with FRP laminates. Different loading conditions, typically adopted in the existing literature, were considered separately, namely: (1) quasi-static compressive axial load only, (2) quasi-static eccentric axial load, and (3) constant axial load and quasi-static lateral load (Fig. 4). For each quasi-static analysis, the columns were modeled as cantilever beams with the coarsest mesh possible (i.e., with a single frame FE unless differently required by the presence of cross-sectional changes in the physical specimen). These analyses were performed based on the Newton-Raphson iterative procedure (Bathe 1995) and incremental displacement control, in order to investigate also the postpeak behavior of the models.

The experimental database for this study was collected from the literature in order to emphasize the contribution of internal steel on the confining pressure imposed to the core concrete. This contribution was measured by considering the ratio c_f between the steel and FRP confinement forces, defined as:

$$c_f = \frac{f_{l,\text{steel}} \cdot A_{c,\text{core}}}{f_{l,\text{FRP}} \cdot A_g} \tag{9}$$

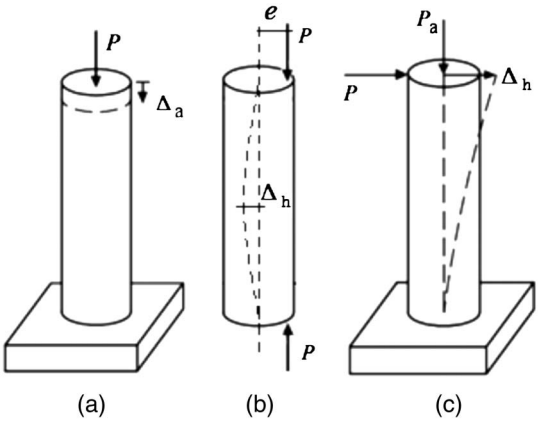

Fig. 4. Loading configurations considered in validation.

in which $A_{c,\text{core}}$ denotes the area of the concrete core (i.e., confined by the steel reinforcement) and A_g denotes the gross area of the member cross-section. The experimental results were selected so that the minimum value of c_f for all cases was larger than or equal to 5%, below which the effects of simultaneous confinement by steel and FRP was considered to be negligible (i.e., the mSM model effectively reduces to the SM model).

Columns Subject to Compressive Axial Load Only

A set of 46 RC columns confined with FRP and subjected to a monotonically increasing and concentrically applied axial load was identified from nine different authors. The description of the selected column specimens' geometry and material properties, as well as the references from which the data were taken, are provided in Table 1. The selected database contains specimens with a wide range of cross-section diameters (from 150 to 400 mm), lengths (from 300 to 2,000 mm), concrete peak strength (from 23.9 to 50.8 MPa), transverse steel reinforcement ratio (from 0.39% to 3.02%), and FRP volume ratio (from 0.22% to 2.01%). The ratio between steel and FRP confinement forces, c_f, varies between 8.3% and 193.6%, with an average value of 40.7%.

Table 2 reports the experimental values and numerical estimates for both the load-carrying capacity and the strain at peak strength for the different FRP-confined RC columns. The numerical estimates obtained by employing the mSM model to describe the mechanical behavior of the core concrete fibers (i.e., those confined by both reinforcing steel and FRP) are also compared to those obtained by using the SM model for the entire cross-section (i.e., neglecting the reinforcing steel's confinement effects) and to those (identified in Table 2 as SM + ΔP_{steel}) obtained by superposing the contributions to the load-carrying capacity due to the FRP confinement (estimated using the SM model) and the steel confinement contribution (ΔP_{steel}), which is estimated based on the relation suggested by Nilson et al. (2009) as

$$\Delta P_{\text{steel}} = 2 \times k_s \times \rho_s \times f_{yt} \times A_{c,\text{core}} \tag{10}$$

in which the k_s coefficient is taken from Mander et al. (1988). The constitutive material model parameters were taken from the data reported in the reference for each set of experiments, whenever the information was available. When some of the information needed to define the model was missing, typical values were used (e.g., the unconfined concrete strain at peak stress ε_{co} was assumed equal to 0.0020, 0.0022, or 0.0024 when the concrete strength was less than 28 MPa, between 28 and 40 MPa, and greater than 40 MPa, respectively, and the parameter β was estimated according to Spoelstra and Monti 1999). Table 2 reports also the ratio between the numerical results and the experimental estimates for both maximum axial load and strain at peak strength for all specimens, as well as the global statistics of these ratios in terms of sample means (μ), coefficients of variations (COV), minima, and maxima for both models considered in this study. The same global statistics were also reported for the estimates of the maximum axial loads obtained by superposing the FRP and steel confinement effects.

It is observed that, on average, the mSM model provides excellent estimates of the columns' maximum axial load capacity, with $\mu = 1.00$ and (i.e., in average the model predicts exactly the columns' axial strength) and COV = 0.10, which indicates a small dispersion of the results. The minimum and maximum values of the numerical to experimental axial strength are 0.68 and 1.15, respectively, which indicate that the mSM model can sometimes significantly underestimate the axial strength of the FRP-confined columns. The SM model produces less accurate and slightly more

Table 1. Experimental test database for FPR-confined RC columns subjected to concentric axial loading: specimens' identification, geometry, and material properties

References	Identifer	d (mm)	L (mm)	f_c (MPa)	f_{yt} (MPa)	f_y (MPa)	ρ_s (%)	ρ_f (%)	E_f (GPa)	σ_f (MPa)	ξ_f	c_f (%)
Parretti and Nanni (2002)	DB450-C	200	914	25.5	517	393	1.42	0.54	126	1,689	0.45	45.7
Matthys et al. (2006)	K2	400	2,000	32	560	620	0.39	0.59	198	2,600	0.61	8.3
	K3	400	2,000	32	560	620	0.39	0.94	480	1,100	1.14	12.3
	K4	400	2,000	32	560	620	0.39	1.8	60	780	0.58	9.0
	K5	400	2,000	32	560	620	0.39	0.6	60	780	0.62	27.1
	K8	400	2,000	32	560	620	0.39	0.49	120	1,100	0.55	23.5
Eid et al. (2009)	A1NP2C	303	1,200	31.7	602	486	2.49	1.01	78	1,050	0.67	87.7
	A3NP2C	303	1,200	31.7	602	550	1.6	1.01	78	1,050	0.60	50.5
	A5NP2C	303	1,200	29.4	602	423	0.75	1.01	78	1,050	0.33	15.9
	C4NP2C	303	1,200	31.7	456	423	1.59	1.01	78	1,050	0.46	40.3
	C4NP4C	303	1,200	31.7	456	423	1.59	2.01	78	1,050	0.89	20.2
	B4NP2C	303	1,200	31.7	456	550	1.59	1.01	78	1,050	0.78	33.3
	C4MP2C	303	1,200	50.8	456	423	1.59	1.01	78	1,050	0.56	40.3
	C2NP2C	303	1,200	31.7	456	423	2.44	1.01	78	1,050	0.43	67.3
	C2N1P2C	303	1,200	36	456	423	2.44	1.01	78	1,050	0.49	67.3
	C2N1P4C	303	1,200	36	456	423	2.44	2.01	78	1,050	0.63	33.6
	C2MP2C	303	1,200	50.8	456	423	2.44	1.01	78	1,050	0.64	67.3
	C2MP4C	303	1,200	50.8	456	423	2.44	2.01	78	1,050	0.80	33.6
Lee et al. (2010)	S2F1	150	300	36.2	1,200	—	3.02	0.29	250	4,510	0.42	193.6
	S2F2	150	300	36.2	1,200	—	3.02	0.59	250	4,510	0.42	96.8
	S2F3	150	300	36.2	1,200	—	3.02	0.88	250	4,510	0.36	64.5
	S2F4	150	300	36.2	1,200	—	3.02	1.17	250	4,510	0.36	48.4
	S2F5	150	300	36.2	1,200	—	3.02	1.47	250	4,510	0.33	38.7
	S4F1	150	300	36.2	1,200	—	1.51	0.29	250	4,510	0.31	88.9
	S4F2	150	300	36.2	1,200	—	1.51	0.59	250	4,510	0.33	44.4
	S4F3	150	300	36.2	1,200	—	1.51	0.88	250	4,510	0.31	29.6
	S4F4	150	300	36.2	1,200	—	1.51	1.17	250	4,510	0.35	22.2
	S4F5	150	300	36.2	1,200	—	1.51	1.47	250	4,510	0.35	17.8
	S6F1	150	300	36.2	1,200	—	1.01	0.29	250	4,510	0.22	54.0
	S6F2	150	300	36.2	1,200	—	1.01	0.59	250	4,510	0.38	27.0
	S6F4	150	300	36.2	1,200	—	1.01	1.17	250	4,510	0.31	13.5
	S6F5	150	300	36.2	1,200	—	1.01	1.47	250	4,510	0.27	10.8
Demers and Neale (1999)	U25-2	300	1,200	23.9	400	400	1.07	1.2	84	1,270	0.38	10.4
	U40-4	300	1,200	43.7	400	400	1.07	1.2	84	1,270	0.22	10.7
Wang et al. (2012)	C1H2L1M	305	915	47	397	340	1.05	0.22	244	4,340	0.79	30.5
	C1H2L2M	305	915	24.5	397	340	1.05	0.44	244	4,340	0.89	15.2
	C1H1L1M	305	915	24.5	397	340	0.53	0.22	244	4,340	0.81	12.9
	C1H1L1C	305	915	24.5	397	340	0.53	0.22	244	4,340	0.81	12.9
	C2H2L1M	204	612	24.5	397	312	1.05	0.33	244	4,340	0.73	16.8
	C2H2L1C	204	612	24.5	397	312	1.05	0.33	244	4,340	0.85	16.8
Cairns (2001)	#28	356	1,524	29.8	510	402	0.56	1.12	82.3	1,770	0.41	10.4
Jaffry (2001)	#16	356	1,524	29.8	510	402	0.56	1.12	45.2	1,070	0.48	17.2
Carrazedo and Hanai (2006)	C2S25	190	570	28.9	756	554.8	1.96	0.55	219	2,801	0.85	65.2
	C2S50	190	570	26.2	756	554.8	0.98	0.55	219	2,801	0.70	29.9
	C1S25	190	570	28.9	756	554.8	1.96	0.27	219	2,801	0.85	130.5
	C1S50	190	570	26.2	756	554.8	0.98	0.27	219	2,801	0.88	59.8

disperse results than the mSM model, with $\mu = 0.88$ and COV $= 0.15$. In particular, the SM model tends to underestimate the axial load capacity of the specimens, which is consistent with the fact that it neglects the effects of steel confinement. This result is also confirmed by the minimum and maximum values of the numerical to experimental axial strength obtained using the SM model, which are 0.55 and 1.08, respectively. Conversely, both models provide practically identical estimates of the strain at peak strength, which slightly overestimate the experimental results ($\mu = 1.07$ for both models) and present a significantly larger dispersion of the results when compared to the axial strength estimates (COV $= 0.23$). This result was also expected, because the numerical prediction of the strain at peak strength is inherently more complex and more affected by uncertainties than the numerical prediction of the peak axial strength (e.g., due to uncertainties/potential inaccuracies in the experimental measurements and the lack of accurate measurements of modeling parameters that affect the numerical prediction of the strains). The results obtained considering a linear superposition of the effects of FRP and steel confinement tend to overestimate the columns' axial load capacity by approximately 10% on average ($\mu = 1.10$), with a dispersion that is similar to that observed for the mSM results (COV $= 0.10$). This observation implies that using Eq. (10) to estimate the steel confinement effect of FRP-confined RC columns subject to concentric axial loads overestimates this effect by a factor approximately equal to 2. The reasons for this overestimation are that (1) the maximum capacity corresponding to each confining mechanism is achieved at different levels of strains, and (2) the linear combination of the FRP and steel confinement effects does not provide a realistic description of the highly nonlinear behavior of the confined RC columns, particularly near the peak strength region.

Table 2. Comparison between experimental results and numerical simulation with both models of load-carrying capacity of RC column specimens subjected to concentric axial loading

	Maximum axial load (kN)							Axial strain at peak strength (mm/m)				
Identifer	Experimental	mSM model	Ratio	SM model	Ratio	SM + ΔP_{steel}	Ratio	Experimental	mSM model	Ratio	SM model	Ratio
DB450-C	1,715	1,692	0.99	1,502	0.88	1,834	1.07	14.9	14.6	0.98	14.6	0.98
K2	7,460	7,969	1.07	7,744	1.04	8,091	1.08	11.1	10.4	0.94	10.4	0.94
K3	7,490	7,542	1.01	7,455	1.00	7,802	1.04	4.3	4.8	1.12	4.8	1.12
K4	7,580	7,723	1.02	7,458	0.98	7,805	1.03	6.9	9.6	1.39	9.5	1.38
K5	7,580	7,723	1.02	7,458	0.98	7,805	1.03	6.9	9.6	1.39	9.5	1.38
K8	6,230	6,263	1.01	5,930	0.95	6,277	1.01	5.9	5.8	0.98	5.8	0.98
A1NP2C	4,571	5,120	1.12	4,106	0.90	5,717	1.25	15	12.3	0.82	12.3	0.82
A3NP2C	4,331	4,744	1.10	4,095	0.95	5,023	1.16	12.5	11	0.88	11	0.88
A5NP2C	3,326	3,558	1.07	3,333	1.00	3,626	1.09	6.3	6.3	1.00	6.3	1.00
C4NP2C	3,704	4,164	1.12	3,731	1.01	4,474	1.21	7.7	8.3	1.08	8.3	1.08
C4NP4C	5,468	5,765	1.05	5,515	1.01	6,258	1.14	20.8	22.7	1.09	22.7	1.09
B4NP2C	4,182	4,776	1.14	4,404	1.05	5,017	1.20	13.6	11.5	0.85	11.5	0.85
C4MP2C	5,434	5,869	1.08	5,364	0.99	6,107	1.12	8.8	8.8	1.00	8.8	1.00
C2NP2C	4,034	4,278	1.06	3,663	0.91	4,899	1.21	8.1	6.5	0.80	6.5	0.80
C2N1P2C	4,502	4,816	1.07	4,080	0.91	5,316	1.18	11	7.8	0.71	7.8	0.71
C2N1P4C	5,459	5,856	1.07	5,310	0.97	6,546	1.20	17.5	13	0.74	13	0.74
C2MP2C	5,689	6,308	1.11	5,496	0.97	6,732	1.18	10.4	8.5	0.82	8.5	0.82
C2MP4C	7,062	7,770	1.10	7,208	1.02	8,444	1.20	15.9	13.8	0.87	13.8	0.87
S2F1	1,255	1,354	1.08	767.9	0.61	1,819	1.45	39	33.3	0.85	33.3	0.85
S2F2	1,590	1,558	0.98	1,045	0.66	2,096	1.32	36	45.3	1.26	45.3	1.26
S2F3	1,873	1,627	0.87	1,194	0.64	2,245	1.20	34	44.6	1.31	44.6	1.31
S2F4	2,015	1,741	0.86	1,351	0.67	2,402	1.19	38	50.6	1.33	50.6	1.33
S2F5	2,651	1,793	0.68	1,446	0.55	2,497	0.94	43	50	1.16	50	1.16
S4F1	1,025	1,053	1.03	718.9	0.70	1,201	1.17	19	23.3	1.23	23.3	1.23
S4F2	1,343	1,265	0.94	979.5	0.73	1,462	1.09	23	34	1.48	34	1.48
S4F3	1,572	1,384	0.88	1,144	0.73	1,627	1.03	29	37.3	1.29	37.3	1.29
S4F4	1,820	1,561	0.86	1,342	0.74	1,825	1.00	30	49	1.63	49	1.63
S4F5	2,209	1,661	0.75	1,473	0.67	1,956	0.89	36	54	1.50	54	1.50
S6F1	901.2	887.7	0.99	678.6	0.75	973	1.08	17	16	0.94	16	0.94
S6F2	1,202	1,216	1.01	1,016	0.85	1,310	1.09	25	40	1.60	40	1.60
S6F4	1,696	1,432	0.84	1,292	0.76	1,586	0.94	34	42	1.24	42	1.24
S6F5	1,767	1,483	0.84	1,364	0.77	1,658	0.94	36	39.3	1.09	39.3	1.09
U25-2	2,950	3,340	1.15	3,180	1.08	3,451	1.17	10	9	0.90	9	0.90
U40-4	4,650	4,950	1.08	4,783	1.03	5,063	1.09	5.9	5	0.85	5	0.85
C1H2L1M	3,726	3,666	0.98	3,329	0.89	3,810	1.02	23.1	19.5	0.84	19.5	0.84
C1H2L2M	4,807	4,663	0.97	4,457	0.93	4,938	1.03	32.9	29.8	0.91	29.8	0.91
C1H1L1M	3,338	3,497	1.05	3,348	1.00	3,554	1.06	18.3	20	1.09	20	1.09
C1H1L1C	3,445	3,503	1.02	3,358	0.97	3,558	1.03	19.6	20.3	1.04	20.3	1.04
C2H2L1M	1,837	1,810	0.99	1,705	0.93	1,883	1.02	25.3	21.2	0.84	21.2	0.84
C2H2L1C	1,992	1,873	0.94	1,775	0.89	1,953	0.98	28	25.2	0.90	25.2	0.90
#28	7,329	6,736	0.92	6,070	0.83	6,532	0.89	18.8	15.5	0.82	15.5	0.82
#15	6,020	6,238	1.04	5,276	0.88	5,738	0.95	16.7	15	0.90	15	0.90
C2S25	2,097	2,102	1.00	1,795	0.86	2,473	1.18	19.2	21.1	1.10	21.1	1.10
C2S50	1,855	1,873	1.01	1,693	0.91	2,004	1.08	15.8	16.5	1.04	16.5	1.04
C1S25	1,692	1,836	1.09	1,409	0.83	2,087	1.23	16.5	15.6	0.95	15.6	0.95
C1S50	1,482	1,531	1.03	1,344	0.91	1,655	1.12	11.6	18.9	1.63	18.9	1.63
Mean	—	—	1.00	—	0.88	—	1.10	—	—	1.07	—	1.07
COV	—	—	0.10	—	0.15	—	0.10	—	—	0.23	—	0.23
Min	—	—	0.68	—	0.55	—	0.89	—	—	0.71	—	0.71
Max	—	—	1.15	—	1.08	—	1.45	—	—	1.63	—	1.63

Fig. 5 plots the experimental and numerical axial force-axial strain responses for two select columns, i.e., specimens DB450-C (Parretti and Nanni 2002) and S2F1 (Lee et al. 2010), for which the coefficients c_f assume the values 45.7% (i.e., close to the average value for the specimens considered here) and 193.6% (i.e., the largest value in the considered database), respectively. In both cases, it is observed that the mSM model, which explicitly accounts for the simultaneous confinement of steel and FRP on the core concrete, shows a better agreement with the experimental results than the SM model not only in terms of the peak strength of the column, but also for the entire axial force-axial strain response curve up to and beyond the failure of the FRP confinement. As expected, the improvement in the experimental results' prediction from the SM to the mSM model is more evident for increasing values of c_f.

Columns Subject to Eccentric Axial Load

A set of 22 specimens of RC columns subjected to monotonically increasing eccentric axial loads was collected from five different authors. In order to accurately account for second-order effects produced by the eccentricity of the load, the FE analysis was

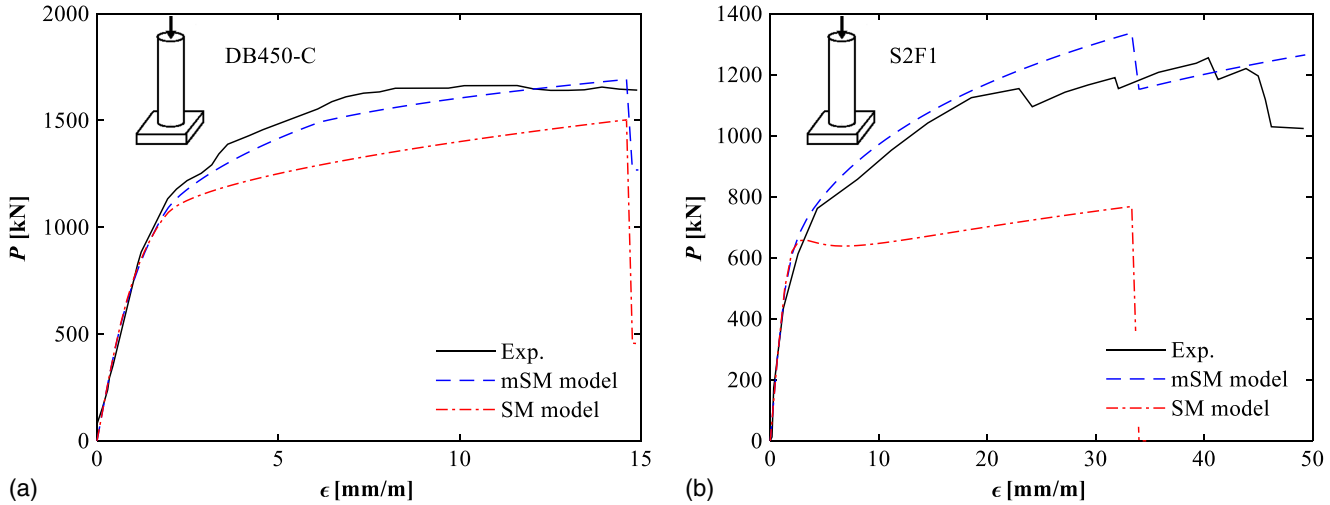

Fig. 5. Comparison between the analytical concrete models and test results for specimens subject to concentric axial load: (a) DB450-C (data from Parretti and Nanni 2002); and (b) S2F1 (data from Lee et al. 2010).

Table 3. Experimental test database for FPR-confined RC columns subjected to eccentric axial loading: specimens' identification, geometry, and material properties

References	Identifer	d (mm)	L (mm)	f_c (MPa)	f_{yt} (MPa)	f_y (MPa)	ρ_s (%)	ρ_f (%)	E_f (GPa)	σ_f (MPa)	c_f (%)
Hadi (2006)	C2	150	620	32	500	500	4.76	2.67	25	700	55.7
Hadi (2009)	CF-25	205	925	75	437	640	3.17	3.08	45.8	884.6	28.9
	CF-50	205	925	75	437	640	3.17	3.08	45.8	884.6	28.9
Bisby and Ranger (2010)	C-5	152	608	33.2	710	710	1.26	1.00	90	894	13.2
	C-10	152	608	33.2	710	710	1.26	1.00	90	894	13.2
	C-20	152	608	33.2	710	710	1.26	1.00	90	894	13.2
	C-30	152	608	33.2	710	710	1.26	1.00	90	894	13.2
	C-40	152	608	33.2	710	710	1.26	1.00	90	894	13.2
Fitzwilliam and Bisby (2010)	300C10A	152	300	30.5	693	710	1.26	1.00	88.2	1,014	11.5
	300C10B	152	300	30.5	693	710	1.26	1.00	88.2	1,014	11.5
	300C20B	152	300	30.5	693	710	1.26	1.00	88.2	1,014	11.5
	600C10A	152	600	30.5	693	710	1.26	1.00	88.2	1,014	11.5
	900C10A	152	900	30.5	693	710	1.26	1.00	88.2	1,014	11.5
	1200C10A	152	1,200	30.5	693	710	1.26	1.00	88.2	1,014	11.5
	1200C10B	152	1,200	30.5	693	710	1.26	1.00	88.2	1,014	11.5
	1200C20A	152	1,200	30.5	693	710	1.26	1.00	88.2	1,014	11.5
	300C12A	152	300	30.5	693	710	1.26	1.00	88.2	1,014	11.5
	1200C12A	152	1,200	30.5	693	710	1.26	1.00	88.2	1,014	11.5
	1200C14A	152	1,200	30.5	693	710	1.26	1.00	88.2	1,014	11.5
Mostofinejad and Moshiri (2014)	IW-30	150	500	28	502	502	2.15	0.45	230	3,900	9.8
	IW-60	150	500	28	502	502	2.15	0.45	230	3,900	9.8
	IW-90	150	500	28	502	502	2.15	0.45	230	3,900	9.8

performed considering the nonlinear geometry conditions based on a P-Δ formulation (Filippou and Fenves 2004). The description of these specimens is given in Table 3, whereas Table 4 provides the comparison between experimental results and numerical estimates obtained using both SM and mSM models, including the means, COVs, minima, and maxima for each model. The experimental specimens include circular columns with cross-section diameters ranging between 150 and 205 mm; length between 300 and 1,200 mm; concrete peak strength between 28 and 75 MPa; transverse steel reinforcement ratio between 1.26% and 4.76%; and FRP volume ratio between 0.45% and 3.08%. The ratio between steel and FRP confinement forces, c_f, varies between 9.8% and 55.7%, with an average value of 15.3%. The last three listed specimens from Fitzwilliam and Bisby (2010) presented longitudinal FRP reinforcement in addition to FRP confinement and were modeled using the FE proposed in Barbato (2009). The specimens from Mostofinejad and Moshiri (2014) were wrapped with discontinuous rings of FRP sheets. The results presented in Table 4 show that both SM and mSM models are able to predict accurately the load-carrying capacity of FRP-confined columns under a combination of a compressive axial load and the bending moment induced by load eccentricity, with a small improvement from a mean ratio of numerical to experimental strength equal to 0.97 for the mSM model and to 0.94 for the SM model. In addition, the COVs of the numerical to experimental strength ratio are also almost the same for the two models, i.e., 0.08 and 0.09 for the mSM and SM models, respectively. Thus, the differences between the two models for this loading case are significantly smaller than the differences observed for the concentric axial load case. This results can be explained as follows: (1) the experimental database of specimens

Table 4. Comparison between experimental results and numerical simulation with both models of load-carrying capacity of RC column specimens subjected to eccentric axial loading

	Maximum axial load (kN)				
Identifer	Experimental	mSM model	Ratio	SM model	Ratio
C2	409	404	0.99	373	0.91
CF-25	2,345	2,377	1.01	2,215	0.94
CF-50	1,372	1,438	1.05	1,387	1.01
C-5	770	828	1.08	795	1.03
C-10	664	708	1.07	691	1.04
C-20	579	575	0.99	557	0.96
C-30	337	361	1.07	360	1.07
C-40	264	246	0.93	246	0.93
300C10A	672	604	0.90	587	0.87
300C10B	683	640	0.94	620	0.91
300C20B	911	912	1.00	902	0.99
600C10A	561	498	0.89	490	0.87
900C10A	549	522	0.95	507	0.92
1200C10A	449	455	1.01	447	1.00
1200C10B	480	449	0.94	444	0.93
1200C20A	537	494	0.92	482	0.90
300C12A	681	622	0.91	604	0.89
1200C12A	582	501	0.86	481	0.83
1200C14A	671	529	0.79	479	0.71
IW-30	544	602	1.11	592	1.09
IW-60	279	269	0.96	265	0.95
IW-90	168	154	0.92	152	0.91
Mean	—	—	0.97	—	0.94
COV	—	—	0.08	—	0.09
Min	—	—	0.79	—	0.71
Max	—	—	1.11	—	1.09

subject to eccentric axial loads contains specimens with significantly smaller amounts of transverse steel than the database available for specimens subject to concentric axial loads, as demonstrated by the smaller average value of c_f (i.e., 15.3% for the case of eccentric axial loads, compared to 42.2% for the case of concentric axial loads); and (2) the presence of a bending moment induced by the eccentricity of the load produces a nonuniform compression or even some tension within the specimen's cross-section, which reduces the effectiveness of the passive confining mechanism of both steel and FRP.

Fig. 6 compares the experimental and numerical response (i.e., axial force versus displacement at midheight) using both mSM and SM concrete constitutive models for specimens 900C10A (Fitzwilliam and Bisby 2010) and C2 (Hadi 2006), for which the coefficients c_f assume the values 11.5% (i.e., close to the average value for the specimens considered here) and 55.7% (i.e., the largest value in the considered database), respectively. The following is observed: (1) for specimen 900C10A ($c_f = 11.5\%$), the two concrete constitutive models provide almost the same results in terms of peak axial strength and ultimate displacement at midheight; and (2) for specimen C2 ($c_f = 55.7\%$), the mSM model provides significantly improved estimates of the peak strength and of the displacement at failure when compared to the corresponding results obtained using the SM model. This result indicates that the internal steel's confinement can significantly affect the response of FRP-confined columns subject to eccentric axial loads when the amount of transverse steel reinforcement is sufficiently large relatively to the amount of FRP, as measured by the coefficient c_f. It is also observed that, for both specimens, the axial load–midheight displacement responses obtained using the FE models present nonnegligible differences with the experimental results. These differences may be due to (1) the complexity of the experimental setup for these eccentric axial load tests, which may affect the accuracy of the experimental displacement results; (2) the approximations of the P-Δ formulation, which considers only some of the nonlinear geometry effects that are affecting the response of these specimens; and (3) the presence of complex 3D nonlinear behavior in the concrete, e.g., triaxial stress conditions and concrete dilation (Cao et al. 2018; Kabir and Shafei 2012), that cannot be accurately represented by a simplified fiber-section frame model.

Columns Subject to Axial and Lateral Loads

A set of 18 FRP-confined RC columns subjected to a constant axial load, P_a, and a cyclic lateral displacement was selected from seven different published works. These specimens are described in Table 5. The considered specimens consist of columns with cross-section diameters varying between 300 and 760 mm, lengths between 850 and 2,000 mm, concrete peak strength between 18.6 and 44.8 MPa, transverse steel reinforcement ratio between 0.13% and 2.22%, FRP volume ratio between 0.11% and 4.06%, and ratio between axial load and cross-section capacity (i.e., P_a/P_o, where P_o corresponds

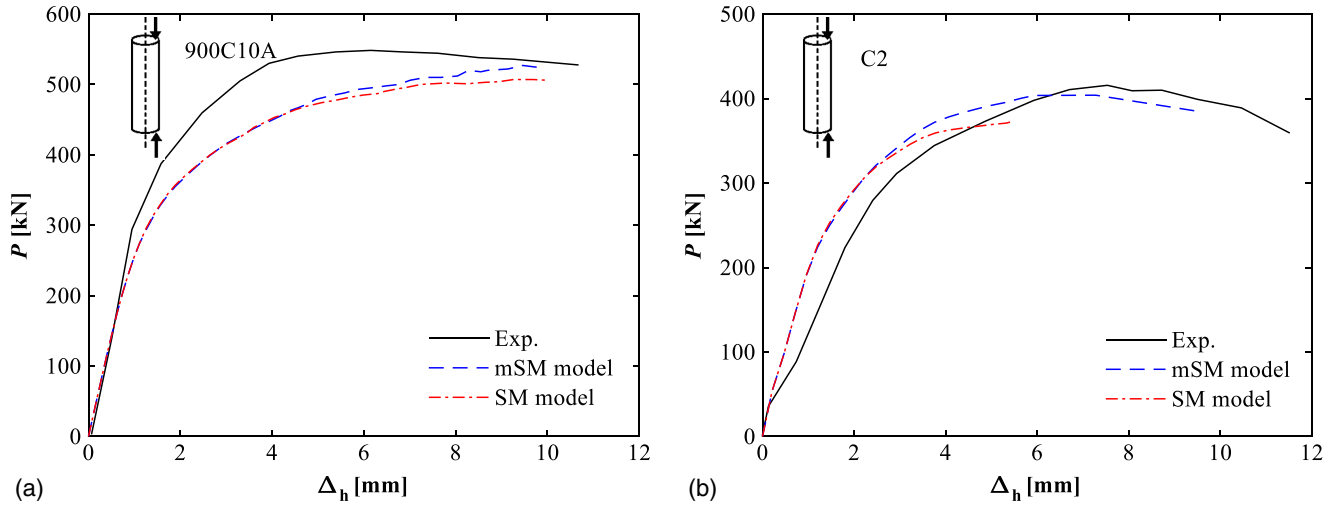

Fig. 6. Comparison between the analytical concrete models and test results for specimens subject to eccentric axial load: (a) 900C10A (data from Fitzwilliam and Bisby 2010); and (b) C2 (data from Hadi 2006).

Table 5. Experimental test database for FPR-confined RC columns subjected to axial and lateral loads: specimens' identification, geometry, and material properties

References	Identifer	d (mm)	L (mm)	f_c (MPa)	P_a/P_o	f_{yt} (MPa)	f_y (MPa)	d_b (mm)	ρ_s (%)	ρ_f (%)	E_f (GPa)	σ_f (MPa)	ξ_f	c_f (%)
Kawashima et al. (2000)	A2	400	1,350	30	0.05	296	296	16	0.23	0.11	243	4,277	0.64[a]	6.1
Li and Sung (2004)	FCS-2	760	1,750	18.6	0.11	426	426	19.6	0.13	0.14	232	4,170	0.64[a]	6.7
Paultre et al. (2015)	S75P10C1	305	2,000	36	0.09	470	415	19.6	2.13	1.32	70.6	849	0.91	47.3
	S150P10C1	305	2,000	33.6	0.35	470	415	19.6	1.07	1.32	70.6	849	0.64	16.2
	S75P35C1	305	2,000	33.6	0.1	470	415	19.6	2.13	1.32	70.6	849	0.91	47.3
	S150P35C1	305	2,000	34.6	0.32	470	415	19.6	1.07	1.32	70.6	849	0.76	16.2
Desprez et al. (2013)	P1C	300	2,000	35.8	0.1	470	415	19.5	2.22	4.06	70.6	849	0.61	16.6
	P2C	300	2,000	34.9	0.35	470	415	19.5	2.22	4.06	70.6	849	0.61	16.6
	P3C	300	2,000	34.4	0.1	470	415	19.5	1.11	4.06	70.6	849	0.61	5.7
	P4C	300	2,000	34.3	0.35	470	415	19.5	1.11	4.06	70.6	849	0.61	5.7
Gu et al. (2010)	J1	300	850	28	0.05	350	400	19	0.33	0.34	60	1,832	0.52	6.6
	J2	300	850	28	0.05	350	400	19	0.33	0.15	230	4,232	0.43	6.6
Sheikh and Yau (2002)	ST-2NT	356	1,473	40.4	0.64	450	450	25	0.3	1.4	20	400	0.74[a]	5.8
	ST-4NT	356	1,473	44.8	0.32	450	450	25	0.3	0.56	75	900	0.64[a]	6.4
	ST-5NT	356	1,473	40.8	0.32	450	450	25	0.3	1.4	20	400	0.74[a]	5.8
Liu and Sheikh (2013)	P271CF3	356	1,473	40	0.32	490	496	25	0.3	1.12	76.4	939	0.83	6.2
	P401CF8	356	1,473	40	0.47	490	496	25	0.3	1.12	76.4	939	0.91	6.2
	P401GF9	356	1,473	40	0.47	490	496	25	0.3	1.4	25.5	518	0.82	9.0

[a]Efficiency factor estimated based on Lam and Teng (2004).

to the concrete strength f_c times the gross area A_g) between 5% and 64%. The coefficient c_f varies between 5.7% and 47.3%, with an average value of 13.2%. The efficiency factors for the FRP rupture strain were taken from the experimental data (when available) or estimated according to Lam and Teng (2004) (when not reported in the experimental investigations).

Table 6 reports the comparison of the experimental results with the numerical estimates of the maximum lateral load-carrying capacity and of the ductility obtained using both mSM and SM models. The ductility is measured here by the ductility parameter $\mu_\Delta = \Delta_2/\Delta_{yI}$ (displacement ductility) or $\mu_\varphi = \varphi_2/\varphi_{yI}$ (curvature ductility) (Paultre et al. 2015), which are obtained using an idealized bilinear load-displacement diagram (Sheikh and Khoury 1993). In this study, Δ_2 and φ_2 are conventionally defined as the displacement and curvature, respectively, where the specimens reach the 80% of the maximum lateral capacity in the postpeak response; and Δ_{yI} and φ_{yI} denote the conventional yield displacement and curvature, respectively, corresponding to the intersection between the peak strength's horizontal line and the secant line of the lateral load-lateral displacement/curvature curve passing through the origin and 75% of the peak strength. The usage of the displacement or curvature ductility for different specimens was dictated by

Table 6. Comparison between experimental results and numerical simulation with both models of load-carrying capacity of RC column specimens subjected to axial and lateral loads

	Maximum lateral load (kN)					Ductility				
Identifer	Experimental	mSM model	Ratio	SM model	Ratio	Experimental	mSM model	Ratio	SM model	Ratio
A2	108.5	110.8	1.02	110.0	0.99	10.8[a]	13.3	1.05	12.4	0.99
FCS-2	878.5	835.7	0.95	828.9	0.94	8.8[a]	8.8	1.00	8.8	1.00
S75P10C1	64.0	59.8	0.93	57.0	0.89	14.4[a]	14.4	1.00	12.4	0.86
S150P10C1	65.8	55.9	0.85	55.5	0.84	10.9[a]	10.9	1.00	10.9	1.00
S75P35C1	91.5	76.9	0.84	74.9	0.82	9.5[a]	11.3	1.19	5.1	0.54
S150P35C1	86.0	76.2	0.89	75.3	0.88	8.5[a]	10.7	1.12	6.6	0.69
P1C	65.0	61.9	0.95	60.1	0.92	12.2[a]	12.2	1.00	7.4	0.61
P2C	90.9	83.8	0.92	82.7	0.91	8.3[a]	10.6	1.08	3.4	0.35
P3C	66.2	62.3	0.94	62.0	0.94	10.6[a]	10.6	1.00	7.2	0.68
P4C	85.5	80.4	0.94	79.5	0.93	10.1[a]	8.2	0.81	4.4	0.43
J1	179.2	177.1	0.99	175.4	0.98	9.7[a]	11.2	1.16	11.2	1.16
J2	192.3	172.2	0.90	171.5	0.89	7.5[a]	9.5	1.15	9.5	1.15
ST-2NT	131.0	142.3	1.09	139.0	0.98	12.7[b]	13.9	1.09	12.9	1.01
ST-4NT	131.6	143.9	1.09	142.1	0.99	13.3[b]	10.4	0.78	9.5	0.71
ST-5NT	124.8	144.3	1.16	141.3	0.98	16.2[b]	14.3	0.88	13.3	0.82
P271CF3	118.6	125.7	1.06	125.1	1.05	14.6[b]	12.8	0.88	12.1	0.83
P401CF8	98.7	108.6	1.10	107.6	1.09	17.3[b]	15.5	0.90	14.9	0.86
P401GF9	115.5	97.3	0.84	94.0	0.81	12.3[b]	13.7	1.11	12.7	1.03
Mean	—	—	0.97	—	0.95	—	—	1.01	—	0.82
COV	—	—	0.10	—	0.10	—	—	0.12	—	0.29
Min	—	—	0.84	—	0.81	—	—	0.78	—	0.35
Max	—	—	1.16	—	1.13	—	—	1.19	—	1.16

[a]Displacement ductility.
[b]Curvature ductility.

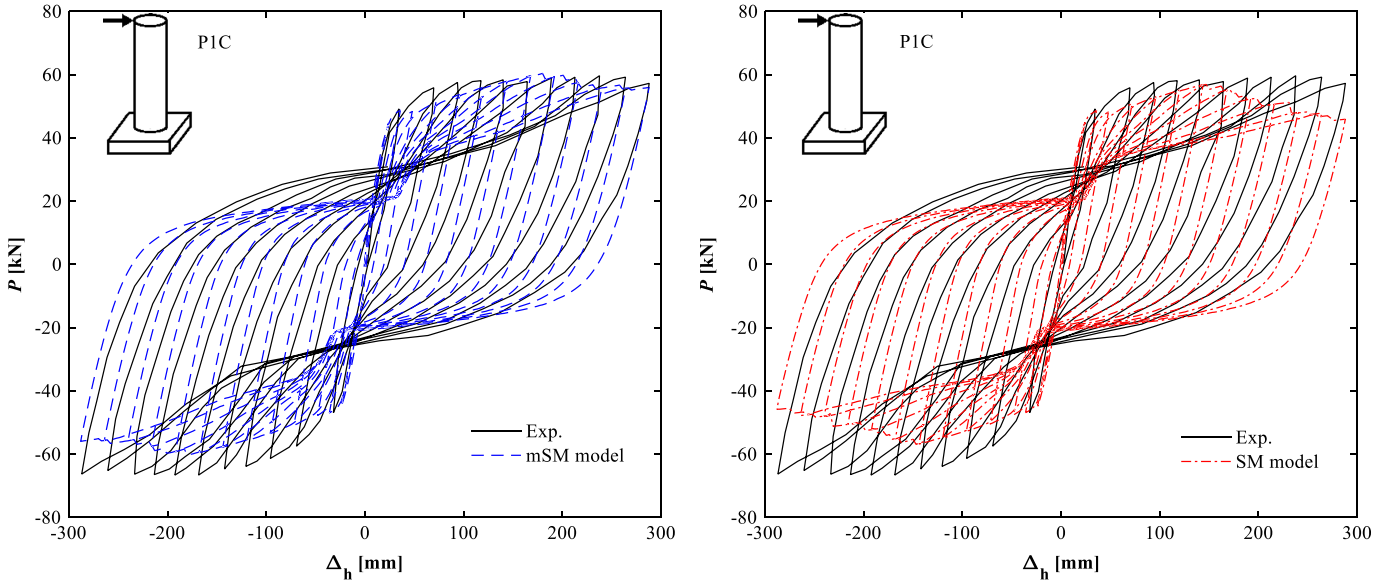

Fig. 7. Comparison between the analytical concrete models and test results for specimen subject to axial and cyclic lateral loads: P1C. (Data from Desprez et al. 2013.)

the manner in which the experimental data were presented in each publication considered in the experimental database.

It is observed that, also for this load case, both mSM and SM models provide very good estimates of the peak lateral load, with a mean equal to 0.97 for the mSM model and to 0.95 for the SM model. The corresponding dispersions are also very similar, i.e., COV = 0.10 for both mSM and SM models. This result is consistent with that obtained for the eccentric axial load case and can be explained in the same way (i.e., small values of c_f and smaller effectiveness of the confinement effect when the columns' cross-sections are not subjected to uniform compression). Due to the limited experimental database available, further investigations will be needed to determine the actual significance of the simultaneous confinement by steel and FRP on the lateral capacity of FRP-confined RC columns.

With respect to the ductility predictions, the mSM model provides results that are in excellent agreement with the experimental results (with $\mu = 1.01$ and COV = 0.12), whereas the SM model tends to underestimate the experimental results and produce a greater dispersion of the ductility estimates (with $\mu = 0.82$ and COV = 0.29). This result seems to indicate that considering the simultaneous confinement of steel and FRP on the core fibers of FRP-confined RC columns could be important for the prediction of their ductility capacity, even if this simultaneous confinement has small or negligible effects on the lateral load capacity. However, additional studies and experimental data are necessary to confirm this preliminary observation, because it is based on a very limited experimental database.

Figs. 7 and 8 compare the experimental and numerical cyclic lateral load-lateral displacement response for two select columns,

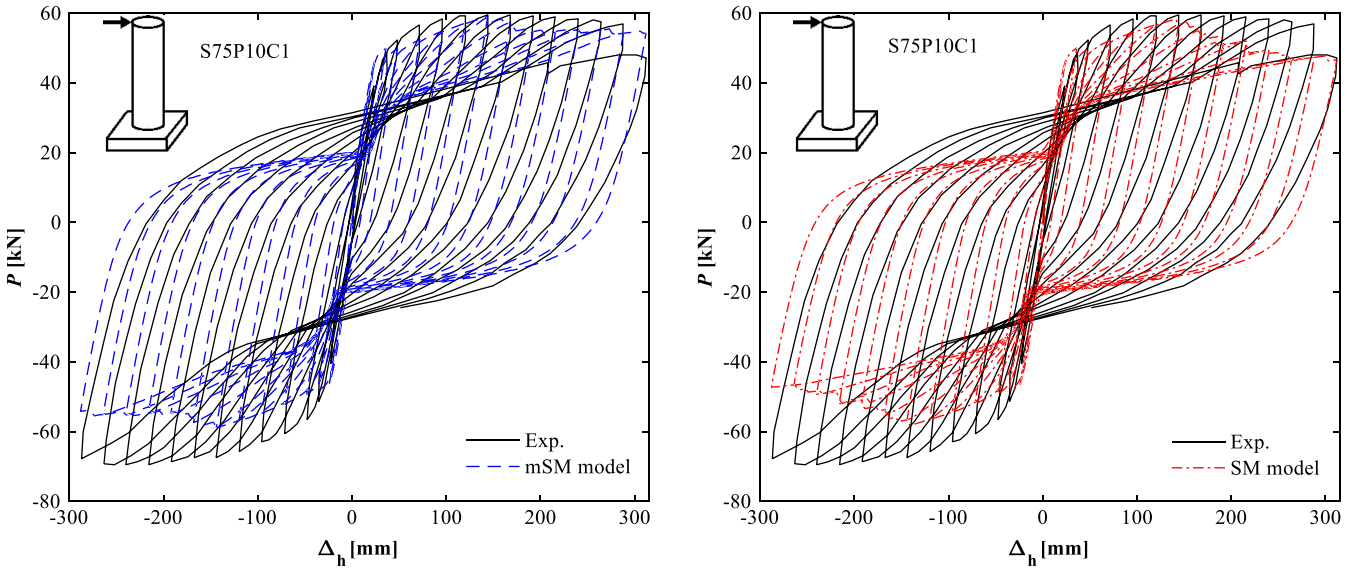

Fig. 8. Comparison between the analytical concrete models and test results for specimen subject to axial and cyclic lateral loads: S75P10C1. (Data from Paultre et al. 2015.)

J. Compos. Constr., 2018, 22(6): 04018064

i.e., specimens P1C (Desprez et al. 2013) and S75P10C1 (Paultre et al. 2015), respectively, for which the coefficients c_f assume the values 16.6% (i.e., close to the average value for the specimens considered here) and 47.3% (i.e., the largest value in the considered database). The results for both specimens indicate that both the mSM and SM models are able to predict the overall cyclic behavior and the lateral load capacity of the specimens; however, the mSM model is also capable to simulate with accuracy the columns' ductile behavior after peak strength, whereas the SM model predicts a strength degradation that is faster than that observed in the experimental results. This result suggests that, for the range of c_f values in the available experimental database, the internal steel's confinement has only a negligible effect on the lateral load capacity, but a larger effect on the lateral ductility capacity of FRP-confined RC columns subjected to a combined loading due to axial and lateral loads.

Conclusions

This paper proposes a new confined concrete material constitutive model that accounts for simultaneous confinement of steel and FRP. The monotonic envelope of the newly proposed model, referred to as modified Spoelstra-Monti (mSM) model, is a modification of the monotonic envelope of the Spoelstra-Monti (SM) model for FRP-confined concrete. Simple hysteresis rules are also proposed to allow the use of the mSM model for cyclic and dynamic loading conditions. This new model is implemented into a research-oriented general-purpose FE program and used in conjunction with a fiber-section force-based frame FE to analyze FRP-confined reinforced concrete columns for which experimental test results are available in the literature. The additional confining effect due to internal reinforcing steel is modeled through the use of the mSM model to characterize the stress-strain behavior of the core concrete's fibers. A new relative confinement coefficient c_f, defined as the ratio of the ultimate reinforcing steel's and FRP's confinement forces in a given cross-section, is proposed as a measure of the internal steel's confinement effects on the response behavior of the FRP-confined columns. Three loading conditions are considered: (1) concentric axial load, (2) eccentric axial load, and (3) a combination of axial load and applied lateral displacement. It is found that the use of the mSM model provides very good agreement with the experimental results, with estimates of the peak strength and axial/lateral deformations that are always more accurate than those obtained using the SM model (i.e., by neglecting the internal reinforcing steel's confinement effect). The internal steel's confinement effect on the peak strength of FRP-confined columns subject to concentric axial loads is significant, whereas the same effect is found to be negligible on the value of the strain at peak strength. The internal steel's confinement effect is found to be small but not negligible for the peak strength of FRP-confined columns subject to eccentric axial load. The same effect appears to be even smaller for the lateral load capacity of FRP-confined columns subject to a combination of axial and lateral loads. However, this effect is larger and could be significant for the lateral ductility capacity of columns under axial and lateral loads. It is noted here that the observations made regarding columns subject to eccentric axial loads and to a combination of axial and lateral loads may require additional investigation to be fully confirmed due to the limited size of the experimental database.

The steel-and-FRP confined concrete model developed in this paper is suitable for use in FE models in conjunction with fiber-section force-based frame FE and can be used for accurate and computationally efficient FE analysis of real-world large-scale structures (e.g., buildings and bridges) with FRP-confined RC columns, for which more accurate 3D FE models could be computationally prohibitive.

Acknowledgments

The authors gratefully acknowledge partial support of this research by the Louisiana Board of Regents (LA BoR) through the Louisiana Board of Regents Research and Development Program, Research Competitiveness (RCS) subprogram, under Award No. LESQSF (2010-13)-RD-A-01; the National Science Foundation through award CMMI #1537078; the Brazilian National Council for Scientific and Technological Development (CNPq—Brazil); and the LASPAU-LSU Fulbright Award. Any opinions, findings, conclusions, or recommendations expressed in this publication are those of the writers and do not necessarily reflect the views of the sponsors.

References

Bakis, C. E., et al. 2002. "Fiber-reinforced polymer composites for construction—State-of-the-art review." *J. Compos. Constr.* 62 (3): 73–87. https://doi.org/10.1061/(ASCE)1090-0268(2002)6:2(73).

Balan, T. A., F. C. Filippou, and E. P. Popov. 1997. "Constitutive model for 3D cyclic analysis of concrete structures." *J. Eng. Mech.* 123 (2): 143–153. https://doi.org/10.1061/(ASCE)0733-9399(1997)123:2(143).

Barbato, M. 2009. "Efficient finite element modelling of reinforced concrete beams retrofitted with fibre reinforced polymers." *Comp. Struct.* 87 (3–4): 167–176. https://doi.org/10.1016/j.compstruc.2008.11.006.

Barbato, M., G. Monti, and F. Santinelli. 2003. "Fiber-section FE of FRP-strengthened RC beam for seismic analysis." In *Proc., Symp. Concrete Structures in Seismic Regions*. Technical Chamber of Greece: Athens, Greece.

Basalo, F. J. C., F. Matta, and A. Nanni. 2012. "Fiber reinforced cement-based composite system for concrete confinement." *Constr. Build. Mater.* 32: 55–65. https://doi.org/10.1016/j.conbuildmat.2010.12.063.

Bathe, K. J. 1995. *Finite element procedures*. Englewood Cliffs, NJ: Prentice-Hall.

Bisby, L., and M. Ranger. 2010. "Axial-flexural interaction in circular FRP-confined reinforced concrete columns." *Constr. Build. Mater.* 24 (9): 1672–1681. https://doi.org/10.1016/j.conbuildmat.2010.02.024.

Cairns, S. W. 2001. "Circular concrete columns externally reinforced with prefabricated carbon polymer shells." Master's thesis, Dept. of Civil Engineering, Univ. of Toronto.

Cao, Y., Y. F. Wu, and C. Jiang. 2018. "Stress-strain relationship of FRP confined concrete columns under combined axial load and bending moment." *Compos. Part B: Eng.* 134: 207–217. https://doi.org/10.1016/j.compositesb.2017.09.063.

Carrazedo, R., and J. Hanai. 2006. "Efeitos do confinamento em pilares de concreto armado encamisados com compósito de fibras de carbono." [In Portuguese.] *Cadernos de Engenharia de Estruturas, São Carlos* 8 (30): 59–77.

Cheng, L., and V. M. Karbhari. 2006. "New bridge systems using FRP composites and concrete: A state of the art review." *Prog. Struct. Eng. Mater.* 8 (4): 143–154. https://doi.org/10.1002/pse.221.

Coleman, J., and E. Spacone. 2001. "Localization issues in force-based frame elements." *J. Struct. Eng.* 127 (11): 1257–1265. https://doi.org/10.1061/(ASCE)0733-9445(2001)127:11(1257).

Demers, M., and K. Neale. 1999. "Confinement of reinforced concrete columns with fibre-reinforced composite sheets—An experimental study." *Can. J. Civ. Eng.* 26 (2): 226–241. https://doi.org/10.1139/l98-067.

Desprez, C., J. Mazars, P. Kotronis, and P. Paultre. 2013. "Damage model for FRP-confined concrete columns under cyclic loading." *Eng. Struct.* 48: 519–531. https://doi.org/10.1016/j.engstruct.2012.09.019.

Eid, R., N. Roy, and P. Paultre. 2009. "Normal- and high-strength concrete circular elements wrapped with FRP composites." *J. Compos. Constr.*

13 (2): 113–124. https://doi.org/10.1061/(ASCE)1090-0268(2009)13:2(113).
Fam, A. Z., and S. H. Rizkalla. 2001. "Confinement model for axially loaded concrete confined by circular fiber-reinforced polymer tubes." *ACI Struct. J.* 98 (4): 451–461. https://doi.org/10.14359/10288.
Fardis, M. N., B. Alibe, and J. L. Tassouas. 1983. "Monotonic and cyclic constitutive law for concrete." *J. Eng. Mech.* 109 (2): 516–536. https://doi.org/10.1061/(ASCE)0733-9399(1983)109:2(516).
Fardis, M. N., and H. H. Khalili. 1982. "FRP-encased concrete as a structural material." *Mag. Concr. Res.* 34 (121): 191–202. https://doi.org/10.1680/macr.1982.34.121.191.
Filippou, F. C., and M. Constantinides. 2004. *FEDEASLab getting started guide and simulation examples*. Technical Rep. NEESgrid-2004-22. Berkeley, CA: Univ. of California Berkeley.
Filippou, F. C., and G. L. Fenves. 2004. "Methods of analysis for earthquake-resistant structures." In *Earthquake engineering from engineering seismology to performance-based engineering*, edited by Y. Bozorgnia and V. V. Bertero, 366–370. Boca Raton, FL: CRC Press.
Filippou, F. C., Popov, E. P., and V. V. Bertero. 1983. *Effects of bond deterioration on hysteretic behavior of reinforced concrete joints*. Rep. No. EERC 83-19. Berkeley, CA: Earthquake Engineering Research Center, Univ. of California.
Fitzwilliam, J., and L. A. Bisby. 2010. "Slenderness effects on circular CFRP confined reinforced concrete columns." *J. Compos. Constr.* 14 (3): 280–288. https://doi.org/10.1061/(ASCE)CC.1943-5614.0000073.
Flaga, K. 2000. "Advances in materials applied in civil engineering." *J. Mater. Process. Technol.* 106 (1): 173–183. https://doi.org/10.1016/S0924-0136(00)00611-7.
Gu, D. S., G. Wu, Z. S. Wu, and Y. F. Wu. 2010. "Confinement effectiveness of FRP in retrofitting circular concrete columns under simulated seismic load." *J. Compos. Constr.* 14 (5): 531–540. https://doi.org/10.1061/(ASCE)CC.1943-5614.0000105.
Hadi, M. N. S. 2006. "Behaviour of FRP wrapped normal strength concrete columns under eccentric loading." *Compos. Struct.* 72 (4): 503–511. https://doi.org/10.1016/j.compstruct.2005.01.018.
Hadi, M. N. S. 2009. "Behaviour of eccentric loading of FRP confined fibre steel reinforced concrete columns." *Constr. Build. Mater.* 23 (2): 1102–1108. https://doi.org/10.1016/j.conbuildmat.2008.05.024.
Hu, D., and M. Barbato. 2014. "Simple and efficient finite element modeling of reinforced concrete columns confined with fiber-reinforced polymers." *Eng. Struct.* 72: 113–122. https://doi.org/10.1016/j.engstruct.2014.04.033.
Hu, H., and R. Seracino. 2014. "Analytical model for FRP-and-steel-confined circular concrete columns in compression." *J. Compos. Constr.* 18 (3): A4013012. https://doi.org/10.1061/(ASCE)CC.1943-5614.0000394.
Ilki, A., O. Peker, E. Karamuk, C. Demir, and N. Kumbasar. 2008. "FRP retrofit of low and medium strength circular and rectangular reinforced concrete columns." *J. Mater. Civ. Eng.* 20 (2): 169–188. https://doi.org/10.1061/(ASCE)0899-1561(2008)20:2(169).
Imran, I., and S. J. Pantazopoulou. 1996. "Experimental study of plain concrete under triaxial stress." *ACI Mater. J.* 93 (6): 589–601. https://doi.org/10.14359/9865.
Ismail, A. M., M. F. M. Fahmy, and Z. Wu. 2017. "Simulating the lateral performance of FRP-confined RC circular columns using a new eccentric-based stress-strain model." *Compos. Struct.* 180: 88–104. https://doi.org/10.1016/j.compstruct.2017.07.075.
Jaffry, S. A. D. 2001. "Concrete-filled glass fiber reinforced polymer (GFRP) shells under concentric compression." Master's thesis, Dept. of Civil Engineering, Univ. of Toronto.
Kabir, M. Z., and E. Shafei. 2012. "Plasticity modeling of FRP-confined circular reinforced concrete columns subjected to eccentric axial loading." *Compos. Part B: Eng.* 43 (8): 3497–3506. https://doi.org/10.1016/j.compositesb.2011.11.075.
Karbhari, V. M., and Y. Gao. 1997. "Composite jacketed concrete under uniaxial compression—Verification of simple design equations." *J. Mater. Civ. Eng.* 9 (4): 185–193. https://doi.org/10.1061/(ASCE)0899-1561(1997)9:4(185).
Kawashima, K., M. Hosotani, and K. Yoneda. 2000. "Carbon fiber sheet retrofit of reinforced concrete bridge piers." In Vol. 2 of *Proc., Int. Workshop on Annual Commemoration of Chi-Chi Earthquake*, 124–135. Taipei, Taiwan: National Center for Research on Earthquake Engineering.
Lam, L., and J. G. Teng. 2004. "Ultimate condition of fiber reinforced polymer-confined concrete." *J. Compos. Constr.* 8 (6): 539–548. https://doi.org/10.1061/(ASCE)1090-0268(2004)8:6(539).
Lee, J. Y., C. K. Yi, H. S. Jeong, and S. W. Kim. 2010. "Compressive response of concrete confined with steel spirals and FRP composites." *J. Compos. Mater.* 44 (4): 481–504. https://doi.org/10.1177/0021998309347568.
Li, Y. F., C. T. Lin, and Y. Y. Sung. 2003. "A constitutive model for concrete confined with carbon fiber reinforced plastics." *Mech. Mater.* 35 (3–6): 603–619. https://doi.org/10.1016/S0167-6636(02)00288-0.
Li, Y. F., and Y. Y. Sung. 2004. "A study on the shear-failure of circular sectioned bridge column retrofitted by using CFRP jacketing." *J. Reinf. Plast. Compos.* 23 (8): 811–830. https://doi.org/10.1177/0731684404032865.
Lin, Y. 2010. "Tension stiffening model for reinforced concrete based on bond stress slip relation." Master's thesis, Dept. of Civil and Environment Engineering, Pennsylvania State Univ.
Liu, J., and S. A. Sheikh. 2013. "Fiber-reinforced polymer-confined circular columns under simulated seismic loads." *ACI Struct. J.* 110 (6): 941–952. https://doi.org/10.14359/51686150.
Mander, J. B., M. J. N. Priestley, and R. Park. 1988. "Theoretical stress-strain model for confined concrete." *J. Struct. Eng.* 114 (8): 1804–1826. https://doi.org/10.1061/(ASCE)0733-9445(1988)114:8(1804).
MathWorks. 1997. "Matlab—High performance numeric computation and visualization software." In *User's guide*. Natick, MA: MathWorks.
Matthys, S., H. Toutanji, and L. Taerwe. 2006. "Stress-strain behavior of large-scale circular columns confined with FRP composites." *J. Struct. Eng.* 132 (1): 123–133. https://doi.org/10.1061/(ASCE)0733-9445(2006)132:1(123).
Menegotto, M., and P. E. Pinto. 1973. "Method of analysis for cyclically loaded reinforced concrete plane frames including changes in geometry and nonelastic behavior of elements under combined normal force and bending." In *Proc., IABSE Symp. on Resistance and Ultimate Deformability of Structures Acted on by Well-Defined Repeated Loads*, 15–22. Zurich, Switzerland: International Association for Bridge and Structural Engineering.
Mertz, D. R., et al. 2003. *Application of fiber reinforced polymer composites to the highway infrastructure*. NCHRP Rep. No. 503. Washington, DC: Transportation Research Board.
Mirmiran, A., and M. Shahawy. 1996. "A new concrete-filled hollow FRP composite column." *Compos. Part B: Eng.* 27B (3–4): 263–268. https://doi.org/10.1016/1359-8368(95)00019-4.
Mostofinejad, D., and N. Moshiri. 2014. "Compressive strength of CFRP composites used for strengthening of RC columns: Comparative evaluation of EBR and grooving methods." *J. Compos. Constr.* 19 (5): 04014079. https://doi.org/10.1061/(ASCE)CC.1943-5614.0000545.
Motavalli, M., and C. Czaderski. 2007. "FRP composites for retrofitting of existing civil structures in Europe: State-of-the-art review." In *Proc., Int. Conf. of Composites and Polycon 2007*, 1–10. Arlington, VA: American Composites Manufacturers Association.
Neuenhofer, A., and F. C. Filippou. 1997. "Evaluation of nonlinear frame finite-element models." *J. Struct. Eng.* 123 (7): 958–966. https://doi.org/10.1061/(ASCE)0733-9445(1997)123:7(958).
Nilson, A. H., D. Darwin, and C. Dolan. 2009. *Design of concrete structures*. New York: McGraw-Hill Education.
Pantelides, C. P., J. Gergely, L. D. Reaveley, and V. A. Volnyy. 2000. "Seismic strengthening of reinforced concrete bridge pier with FRP composites." In Vol. 127 of *Proc., 12th World Conf. on Earthquake Engineering*, 1–8. Upper Hutt, NZ: New Zealand Society for Earthquake Engineering.
Parretti, R., and A. Nanni. 2002. "Axial testing of concrete columns confined with carbon FRP: Effect of fiber orientation." In Vol. 8 of *Proc., 3rd International Conference on Composites in Infrastructure*, 1–10. Tucson, AZ: Dept. of Civil Engineering and Engineering Mechanics, Univ. of Arizona.
Paulay, T., and M. J. N. Priestley. 1992. *Seismic design of reinforced concrete and masonry buildings*. New York: Wiley.

Paultre, P., M. Boucher-Trudeau, R. Eid, and N. Roy. 2015. "Behavior of circular reinforced concrete columns confined with carbon fiber-reinforced polymers under cyclic flexure and constant axial load." *J. Compos. Constr.* 20 (3): 04015065. https://doi.org/10.1061/(ASCE)CC.1943-5614.0000624.

Pellegrino, C., and C. Modena. 2010. "Analytical model for FRP confinement of concrete columns with and without internal steel reinforcement." *J. Compos. Constr.* 14 (6): 693–705. https://doi.org/10.1061/(ASCE)CC.1943-5614.0000127.

Popovics, S. 1973. "Numerical approach to the complete stress-strain relation for concrete." *Cem. Concr. Res.* 3 (5): 583–599. https://doi.org/10.1016/0008-8846(73)90096-3.

Saadatmanesh, H., M. R. Ehsani, and M. W. Li. 1994. "Strength and ductility of concrete columns externally reinforced with fiber composite straps." *ACI Struct. J.* 91 (4): 434–447. https://doi.org/10.14359/4151.

Samaan, M., A. Mirmiran, and M. Shahawy. 1998. "Model of concrete confined by fiber composites." *J. Struct. Eng.* 124 (9): 1025–1031. https://doi.org/10.1061/(ASCE)0733-9445(1998)124:9(1025).

Scott, M. H., and G. L. Fenves. 2006. "Plastic hinge integration methods for force-based beam-column elements." *J. Struct. Eng.* 132 (2): 244–252. https://doi.org/10.1061/(ASCE)0733-9445(2006)132:2(244).

Seible, F., M. J. N. Priestley, G. A. Hegemier, and D. Innamorato. 1997. "Seismic retrofit of RC columns with continuous carbon fiber jacket." *J. Compos. Constr.* 1 (2): 52–62. https://doi.org/10.1061/(ASCE)1090-0268(1997)1:2(52).

Shao, Y., Z. Zhu, and A. Mirmiran. 2006. "Cyclic modeling of FRP-confined concrete with improved ductility." *Cement. Concr. Compos.* 28 (10): 959–968. https://doi.org/10.1016/j.cemconcomp.2006.07.009.

Sheikh, S. A., and S. Khoury. 1993. "Confined concrete columns with stubs." *ACI Struct. J.* 90 (4): 414–431. https://doi.org/10.14359/3960.

Sheikh, S. A., and G. Yau. 2002. "Seismic behavior of concrete columns confined with steel and fiber-reinforced polymers." *ACI Struct. J.* 99 (1): 72–80. https://doi.org/10.14359/11037.

Shirmohammadi, F., A. Esmaeily, and Z. Kiaeipour. 2015. "Stress-strain model for circular concrete columns confined by FRP and conventional lateral steel." *Eng. Struct.* 84: 395–405. https://doi.org/10.1016/j.engstruct.2014.12.005.

Spacone, E., F. C. Filippou, and F. F. Taucer. 1996. "Fiber beam-column element for nonlinear analysis of R/C frames. Part I: Formulation." *Earthquake Eng. Struct. Dyn.* 25 (7): 711–725. https://doi.org/10.1002/(SICI)1096-9845(199607)25:7<711::AID-EQE576>3.0.CO;2-9.

Spoelstra, M. R., and G. Monti. 1999. "FRP-confined concrete model." *J. Compos. Constr.* 3 (3): 143–150. https://doi.org/10.1061/(ASCE)1090-0268(1999)3:3(143).

Teng, J. G., Y. L. Huang, L. Lam, and L. P. Ye. 2007. "Theoretical model for fiber-reinforced polymer-confined concrete." *J. Compos. Constr.* 11 (2): 201–210. https://doi.org/10.1061/(ASCE)1090-0268(2007)11:2(201).

Toutanji, H. A. 1999. "Stress-strain characteristics of concrete columns externally confined with advanced fiber composite sheets." *ACI Mater. J.* 96 (3): 397–404. https://doi.org/10.14359/639.

Wang, Z. Y., D. Y. Wang, S. T. Smith, and D. G. Lu. 2012. "Experimental testing and analytical modeling of CFRP-confined large circular RC columns subjected to cyclic axial compression." *Eng. Struct.* 40: 64–74. https://doi.org/10.1016/j.engstruct.2012.01.004.

Xiao, Y., and H. Wu. 2000. "Compressive behavior of concrete confined by carbon fiber composite jackets." *J. Mater. Civ. Eng.* 12 (2): 139–146. https://doi.org/10.1061/(ASCE)0899-1561(2000)12:2(139).